LIP-STUDENTS-25-5

Characterisation of plastic scintillators read by SiPMs

Maria Luísa Mendes[1,a], Tiago Marçal[2,b] , Margarida Barreiro[1,c] , and Sofia Gonçalvesl[1,d]

[1] *Universidade de Coimbra, Coimbra, Faculdade de Ciência e Tecnologias, Portugal*

Universidade da Beira Interior, Covilhã, Faculdade de Engenharia, Portugal

Project supervisor: Alberto Blanco Castro

September 25, 2025

Abstract. In this study, we analysed the performance of a set of scintillation detectors (plastic scintillalors coupled with silicon photomultipliers) in terms of time resolution, detection efficiency, timing differences and charge response to cosmic muons. Several experimental setups were used, including stacked configurations, diferent detector piles and a setup with a Na-22 radioactive source, to extract the timing and efficiency of individual detectors. Time resolutions were obtained by fitting Gaussian functions to the distributions of time differences between detector pairs and solving the resulting system of equations for each detector. Efficiencies were measured using coincidence triggers. The results show that all detectors achieved efficiencies above 0.97, with typical time resolutions on the order of a few nanoseconds that correlate to the sampling area and the SiPM output of each detector.

Keywords: Detector, SiPM, Scintillator, Time Resolution, Average Charge Amplitude, Efficiency

1 Introduction

A Silicon Photomultiplier (SiPM) is a semiconductor based sensor engineered to detect and measure extremely low levels of light, down to the single photon scale. It serves as a solid-state alternative to traditional Photomultiplier Tubes (PMTs), offering similar sensitivity alongside advantages such as compact size, enhanced durability, and reduced operating voltages [1]. Architecturally, a SiPM comprises a matrix of microcells, where each microcell consists of an avalanche photodiode (APD), operating in Geiger mode, connected in series with a quenching resistor; these microcells are then linked in parallel to form the complete sensor [2].When a photon strikes one of the SiPM's microcells, it initiates an electron-hole pair that triggers a breakdown, resulting in a current pulse due to an electron avalanche. The combined output from all microcells produces an analog signal.

Muons (μ^- and μ^+) are fundamental subatomic particles that resemble electrons (e^-), but with a mass approximately 207 times greater. They are continuously produced when high energy cosmic rays mainly protons (p^+) and atomic nuclei traveling near the speed of light ($c \approx 3 \times 10^8$ m/s) collide with atoms in the Earth's atmosphere. Although they have a short lifetime of about 2.2 μs (2.2×10^{-6} s) before decaying into electrons, muons travel at nearly the speed of light making them capable of being detected on Earth's surface (due to time dilation). Muons can also penetrate deeply into matter which makes them valuable probes in various particle detection and imaging applications [3].

In this study, we utilize the detection of cosmic muons as a means to characterize multiple arrangements of plastic scintillators with the same SiPM model. The research is carried out at LIP (Laboratório de Instrumentação e Física Experimental de Partículas), where multiple SiPM models are coupled to plastic scintillator detectors. Our objective is to systematically evaluate the performance of each sensor by subjecting them to a variety of experimental conditions, focusing particularly on their responses to muon events.

Through this characterization process, parameters such as signal amplitude, timing resolution, and detection efficiency will be assessed. The results will enable a comparative analysis of the operational strengths and weaknesses of each type of SiPM, providing detailed information on their suitability for practical detection tasks involving minimum ionizing particles (MIPs) such as muons.

2 Experimental Setup

In Figure 1, the experimental setup used throughout the project is shown. This setup provided the necessary tools to obtain accurate and reliable results.

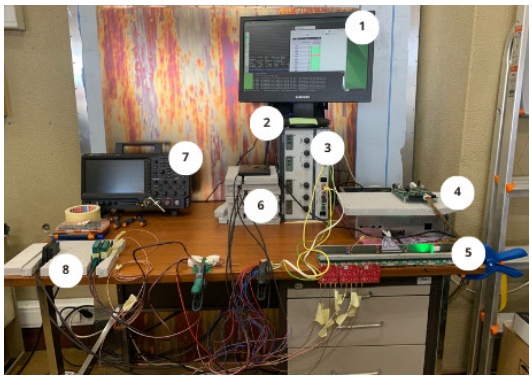

Figure 1. Overview of the full setup: 1. Computer monitor; 2. Router; 3. Power supply; 4. DAQ system; 5. Front End Electronics ; 6. SiPM stack; 7. Oscilloscope; 8. Set of detectors

[a] e-mail: b
[b] e-mail: a
[c] e-mail: a
[d] e-mail: a

2.1 Data Acquisition System

The DAQ system is shown in more detail in Figure 2, with the different components labeled.

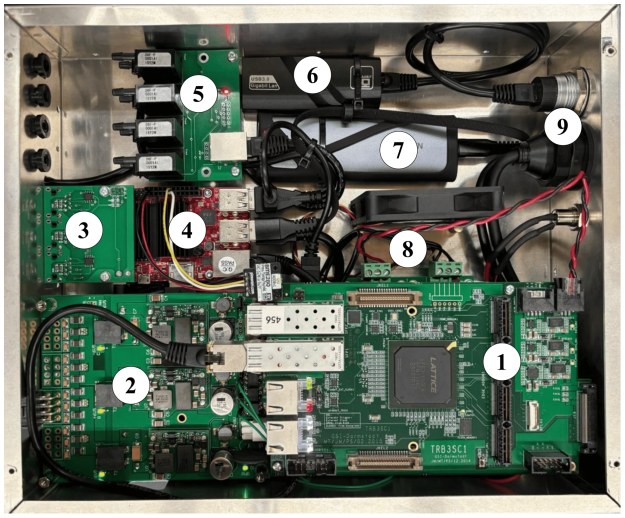

Figure 2. Overview of the Data Acquisition Setup [4]: 1. FPGA Board TRB3SC1; 2. LV Power System; 3. I2C distribution board; 4. Mini-PC; 5. Gas Sensor Module; 6. USB Adapter Ethernet; 7. NVMe M.2 SSD; 8. Relay Control Board; 9. Power and computer connections.

2.2 Private Network Configuration

For the safety of the acquisition process, a private network was established to ensure that data collection could continue uninterrupted, even in the event of an unexpected internet failure. This was made possible by the router labeled as number 2 in Figure 1, an ASUS RT-AX1800 [6].

2.3 SiPM Stack Assembly

The image in Figure 3 shows the two of the main electronic boards used in the Data Acquisition (DAQ) system: the **daughter boards** and the **motherboard**.

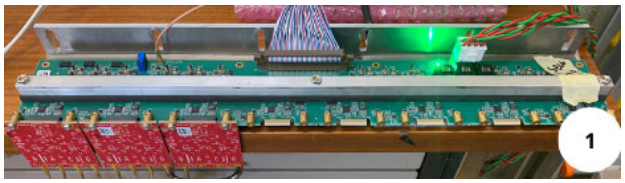

Figure 3. Mother Board and Daughter Board

- **Daughter Boards:** The red modules visible in the image are daughter boards, each connected directly to a Silicon Photomultiplier (SiPM). Their functions include:
  - Receiving analog signals from the SiPMs.
  - Comparing the signal to a fixed threshold using a discriminator.
  - Outputting a digital signal when the input exceeds the threshold.
  - Measuring the charge of the input signal via Time over Threshold (ToT), which correlates with the deposited energy.
- **Motherboard:** The green base board provides infrastructure and control. It:
  - Supplies power to the daughter boards.
  - Contains components to set or adjust the threshold levels.
  - Interfaces with the main DAQ system for data collection and transmission.

Figure 4. Overview of the SiPM Stack

Figure 4 shows the SiPM stack with styrofoam used to hold the scintillators in place during data acquisition. This setup also made it easier to test the efficiency of different scintillators, as they could be repositioned to any desired layer.

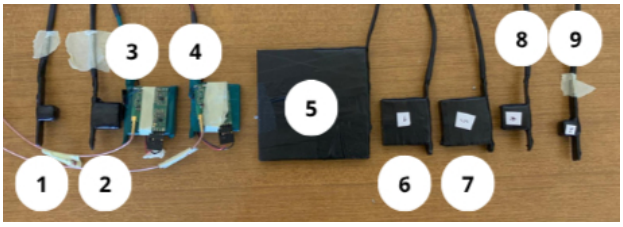

Figure 5. Photograph showing all detectors used in the project, labeled from left to right. Their areas are in centimeters: 1. 1×1; 2. 2×2; 3. 4×4; 4. 4×4; 5. 10×10; 6. 4×4; 7. 4×4; 8. 2×2; 9. 1×1.

Figure 5 shows all detectors used in the project, aligned and labeled with their respective sizes in the caption. Each detector consists of a plastic scintillator coupled with a Silicon Photomultiplier (SiPM). It is important to note that although detectors 3 and 4 have the same SiPM model as the rest, their connection to the DAQ system is made through the fast output of the SiPM. This fast output provides significantly improved timing performance compared to the standard output, enabling ultra-fast signal processing.

3 Procedure

The procedure for obtaining the results involved several steps involving data acquisition, processing and analysis. In order to obtain the characteristics of each detector, parameters such as time resolution, detection efficiency and average charge amplitude were calculated.

3.1 Raw Data Acquisition

The raw data was acquired through the setup shown in Figure 1. When a muon passes through the detector, it deposits energy in the scintillator material. As a result, the scintillator emits photons. These photons are detected by the Silicon Photomultiplier (SiPM). The combined output from all microcells present in the SiPM produces an analog signal, which is then sent to the motherboard and daughter board, whose functions are described in Section 2.3.

Finally, the signal reaches the data acquisition (DAQ) system, shown in Figure 2, where it is digitized, recorded, and processed for further analysis.

3.2 Data Processing

The data processing was carried out using a GitHub repository [5] developed by Alberto Blanco. This software is primarily used to control the DAQ system and proved to be very helpful for both data acquisition and processing.

Focusing on the processing aspect, the software extracts data from files in the `.hld` format and converts them into `.mat` files, which are compatible with MATLAB for further analysis. This conversion is necessary because the raw `.hld` files contain unprocessed data, such as event timestamps, ADC (charge/amplitude), TDC (time), and header information like the run number and setup configuration. These files are not directly readable by MATLAB.

In contrast, the resulting `.mat` files are processed and contain structured data such as the time (`T`) and charge (`Q`) matrices for different detectors. This format allows for immediate use in MATLAB for tasks such as plotting, filtering, and more advanced analyses, including efficiency calculations.

3.3 Data Analysis

The time resolution of each detector was determined by analyzing the timestamps from the detection events recorded across multiple detectors. For every unique pair of detectors, the time differences between their recorded events were calculated and used to obtain histograms. These differences tell us how much the signals from one detector are shifted in time compared to another. The time units are in nanoseconds (ns).

To quantify this shift, a Gaussian function was fitted to each histogram, and the standard deviation (σ) of the fit was obtained. Assuming that the timing uncertainties are independent and normally distributed, the variance of the time difference between any two detectors is equal to the sum of their individual variances:

$$\sigma_{ij}^2 = \sigma_i^2 + \sigma_j^2$$

This relationship was used to construct a system of linear equations, one for each detector pair. The system was then solved to determine the variances (σ^2) of each individual detector and consequently the time resolution (σ) for each detector. In a system composed of 3 detectors this set of equations can be written in matrix form as

$$\begin{bmatrix} 1 & 1 & 0 \\ 1 & 0 & 1 \\ 0 & 1 & 1 \end{bmatrix} \cdot \begin{bmatrix} \sigma_i^2 \\ \sigma_j^2 \\ \sigma_k^2 \end{bmatrix} = \begin{bmatrix} \sigma_{ij}^2 \\ \sigma_{ik}^2 \\ \sigma_{jk}^2 \end{bmatrix}$$

In addition, the time resolution can be further refined by examining how the measured time difference depends on the signal charge amplitude. By fitting the time differences as a function of charge amplitude (using a polynomial function), the dependence of time difference on charge can be removed. The corrected distributions can then be plotted, from which a new σ is extracted, leading to an improved time resolution.

The efficiency of each detector was calculated as the ratio of the number of events that coincide in three detectors (including the scintillator under study) to the number of events coincident in the other two detectors. There are some cases where this parameter is obtained using 4 detectors. The error is given by Poisson statistics.

$$E_j = \frac{N_{ijk}}{N_{ik}}$$

$$\sigma_{E_j} = E_j \cdot \sqrt{\frac{1}{N_{ijk}} + \frac{1}{N_{ik}}}$$

To isolate the data pertaining specifically to muon-related events, two types of triggers were applied. The first trigger (muon trigger) required the event to coincide in two detectors. The second trigger (DT trigger) further restricted this selection by requiring the time difference between events in both detectors to lie within the interval defined by the mean ± one standard deviation (σ) of their Gaussian time difference distribution. Furthermore, in cases where the charge distribution was studied, a cut filter was applied to remove low charge values from the distribution, eliminating noise and ensuring only significant muon-related signals were considered.

4 Results

4.1 Experiment Layout 1

To determine the characteristics of Detector 5 specifically its time resolution, efficiency, and the mean charge deposited by muons Setup 1 was used (as shown in Figure 6). In this configuration, Detector 5 was placed between Detectors 6 and 7, which were symmetrically aligned on either side of it. A total of nine positions were tested, each of which is illustrated in Figure 7).

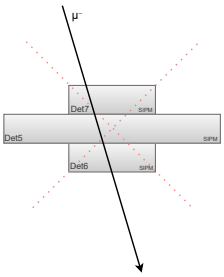

Figure 6. Overview of the SiPM Stack - Setup 1

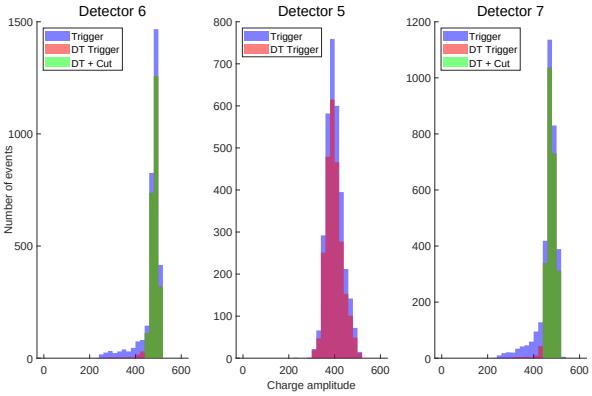

Figure 9. Charge distribution for detector position 1

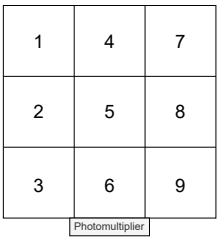

Figure 7. Detector positions

We obtained the time difference distributions between coincident detection events on each pair of detectors, as well as the charge distribution of the events recorded by each detector.

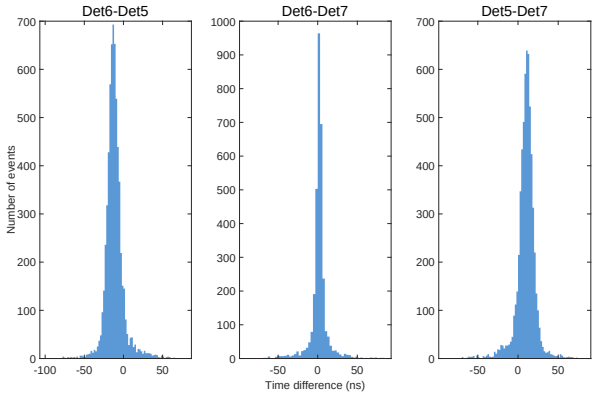

Figure 8. Time differences between detectors for detector position 1

From the set of histograms in Figure 8, we observe that the Gaussian mean of the time differences is close to zero, indicating that the recorded events have similar timing. This is due to the cable size, as the cable that connects each detector to the DAQ system affects the arrival time of detection events.

For the charge distribution of the detection events, the triggers described previously in Section 3.3 (muon trigger, differential time trigger, and cut filter) were applied to isolate muon-induced events. The muon trigger (blue) significantly reduced occurrences with amplitudes below 300 in all detectors and below 400 in detectors 6 and 7. The differential time (DT) trigger (pink) further suppressed low-amplitude events, as shown in Figure 8. Finally, the cut filter (green) removed all remaining low-amplitude occurrences in detectors 6 and 7, although its effect largely overlaps with the DT trigger data. By restricting the charge distribution to muons, we conclude that the charge deposited by muons corresponds to an amplitude of approximately 400–500.

Table 1 and Figure 10 provide an overview of the parameters of the three detectors, with Figure 10 showing the spatial distribution of each parameter for detector 5. The evaluated parameters are time resolution, average charge amplitude, and efficiency. Ideally, the resolution and average charge of detectors 6 and 7 should remain consistent across all positions, however, some disparities are evident, particularly in the resolution values. To address this and improve the data, the dependence of the time differences on charge was removed (as described in Section 3.3), yielding a new value of σ, which is expected to be smaller than the original and consistent between the diferent detector positions.

Regarding detector 5, for positions 1–3 and 7–9, the time resolution worsens as the distance to the SiPM decreases, while for positions 4–6 it gradually improves, reaching a minimum of 5.612. This suggests that, at positions 3 and 9, the light produced in the scintillator does not travel directly to the SiPM but instead undergoes internal reflections before detection. Furthermore, the recorded charge amplitude reaches its maximum at the position closest to the SiPM (position 6), with an average value of 429.215.

Table 1. Summary of detector results.

Parameters	Positions								
	1	2	3	4	5	6	7	8	9
σ_6 (ns)	2.198	1.644	3.077	2.619	2.967	1.925	2.610	2.348	1.966
σ_5 (ns)	6.663	6.964	8.600	6.759	6.048	5.612	6.936	7.435	8.149
σ_7 (ns)	2.588	2.726	2.151	2.834	2.534	2.747	2.926	2.982	3.539
$\sigma_{6,7}$ (ns) (corrected)	1.140	0.990	1.057	1.180	0.924	1.000	0.960	1.046	0.891
Average Q6	470.251	470.148	464.526	463.868	466.552	471.775	464.743	463.580	464.892
Average Q5	399.993	400.913	399.651	393.398	406.633	429.215	394.325	392.134	397.105
Average Q7	464.322	464.091	455.113	457.932	459.270	464.390	458.394	454.423	456.795
Efficiency	0.971	0.968	0.975	0.979	0.983	0.977	0.976	0.982	0.978
Efficiency (DT)	0.988	0.995	0.990	0.991	0.994	0.992	0.991	0.994	0.989

1	4	7
σ5 6.663 Average Q5 399.993 Efficiency 0.971 Efficiency (DT) 0.988	σ5 6.759 Average Q5 393.398 Efficiency 0.979 Efficiency (DT) 0.991	σ5 6.936 Average Q5 394.325 Efficiency 0.976 Efficiency (DT) 0.991
2	**5**	**8**
σ5 6.964 Average Q5 400.913 Efficiency 0.968 Efficiency (DT) 0.995	σ5 6.048 Average Q5 406.633 Efficiency 0.983 Efficiency (DT) 0.994	σ5 7.435 Average Q5 392.134 Efficiency 0.982 Efficiency (DT) 0.994
3	**6**	**9**
σ5 8.600 Average Q5 399.651 Efficiency 0.975 Efficiency (DT) 0.990	σ5 5.612 Average Q5 429.215 Efficiency 0.977 Efficiency (DT) 0.992	σ5 8.149 Average Q5 397.105 Efficiency 0.978 Efficiency (DT) 0.989

Figure 10. Parameters of detector 5

4.2 Experiment Layout 2

Detector	Efficiency ± Error
2	0.9524 ± 0.0722
3	0.9978 ± 0.0464
4	0.9886 ± 0.0566
5	1.0000 ± 0.0205
6	0.9937 ± 0.0457
7	0.9937 ± 0.0457
8	0.9805 ± 0.1123

Table 2. Efficiencies of the 7 Detectors

A second setup was tested, in which all detectors were stacked vertically on top of one another, aligned centrally (as shown in Figure 11) to evaluate their efficiencies and time resolutions. Their efficiencies were obtained using coincident events between 4 detectors.

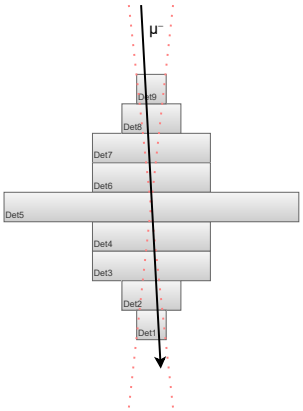

Figure 11. Overview of the SiPM Stack- Setup 2

As expected, all detectors exhibited similar efficiencies, with values around 0.99, which is consistent with the typical performance of this type of detector.

Detector	Average Charge Q	Resolution (ns)
9	412.7879	2.2427
8	453.7613	1.3797
7	376.9429	2.9266
6	379.1820	1.7787
5	342.4781	7.7091
4	281.1178	—
3	299.7581	—
2	476.5386	1.0680
1	463.5494	2.0772

Table 3. Parameters of the Nine Detectors

For Detectors 3 and 4, the method used to resolve individual time resolutions introduces significant errors due to their high resolution, resulting in large uncertainties. To address this, we assume that both detectors contribute equally to the measured time difference and that their timing uncertainties are independent and Gaussian-distributed. Under these conditions, the variance of their time difference is the sum of their individual variances. The time resolution of each detector is then approximated as the standard deviation of their time difference distribution divided by $\sqrt{2}$:

$$\sigma_{det} = \frac{\sigma_{measured}}{\sqrt{2}}$$

Detectors 3 and 4 have both a time resolution of 0.4257.

Additionally, we observe a correlation between charge amplitude and the scintillator area: as the area increases, the average charge amplitude decreases. This effect arises because larger scintillators cause greater light scattering, which in turn reduces the detected charge and its average value.

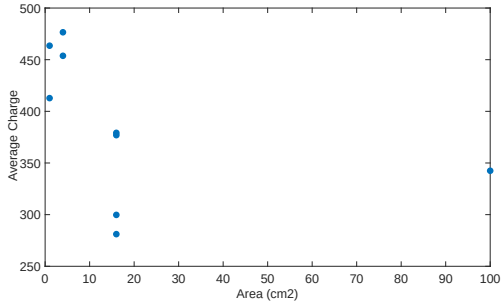

Figure 12. Scintillator Area (cm^2) vs Average Charge

4.3 Experiment Layout 3

Next, the detector stack was divided into two groups: the first consisting of Detectors 2, 3, 4, 6, 7, and 8, with active areas of 4, 16, 16, 16, 16, and 4 cm², respectively; and the second consisting of Detectors 1, 5, and 9, with active areas of 1, 100, and 1 cm², respectively. This configuration was used to measure coincidences between the two groups, as well as to study the dependence of the detected event rate on the separation distance between them.

Detector	Efficiency ± Error
7	0.994 ± 0.079
6	0.991 ± 0.078
4	0.988 ± 0.078
3	0.988 ± 0.078

Table 4. Position 4

Detector	Average Charge Q	Resolution (ns)
9	412.264	—
8	458.055	1.349
7	376.339	3.374
6	377.125	2.411
5	343.783	—
4	277.744	0.388
3	294.048	0.388
2	470.633	1.292
1	460.291	—

Table 5. Parameters for Nine Detectors

By separating the detector stacks, one would expect to observe more events with charges below 400-500 due to electromagnetic showers triggered by muons. In this case, although there are a few events associated with low charges, the majority correspond to higher charges, which are likely muons (as indicated by the muon trigger). These muons create simultaneous events in both stacks, and thus may originate from the same cosmic ray. We could have experimented with different separations between the stacks to analyze this issue further, however, due to time constraints, the setup was tested with only one distance

4.4 Experiment Layout 4

In the final setup, detectors 3, 4, 6, and 7 were paired and positioned vertically at a distance, with a Na-22 source placed between the pairs (these pairs consisted of 6,3 and 4,7). Since detectors 3 and 4 have a faster output, this configuration was used to measure their time resolution. As such, their timing differences and recorded charge amplitude were assessed.

Detector	Resolution (ns)
3,4	1.542
6,7	15.343

Table 6. Resolution for detectors 3,4,6 and 7

For the calculated time resolution shown in Table 6 the previous method where the variance of the time difference is the sum of the individual variances is used . In addition, the charge amplitude measured in each detector is smaller than that induced by muon events, indicating that the positrons emitted by the Na-22 source produce photons (through annihilation) that deposit less energy in the scintillator material compared to muons.

5 Conclusions

In conclusion, during this internship we were able to determine and characterize all nine detectors. All detectors were shown to exhibit high efficiencies ($\approx$ 0.97–0.99) and good time resolutions: around 1–2 ns for detectors 1, 2, 6, 7, 8, and 9; 6–7 ns for detector 5; and 0.5 ns for the fast detectors 3 and 4 for measuring muons , and considerably worse for gammas. We also observed that the average charge is proportional to the scintillator area. Finally, for the large detector 5, both the time resolution and the average charge reach their optimal values right on the SiPM, while the opposite behavior is observed at the extremities of the detectors.

Acknowledgements

We would like to thank our supervisor Alberto Blanco Castro and the team at LIP for this opportunity to enrich our knowledge. Our heartfelt gratitude goes to them for their unwavering support and insightful guidance. This internship gives us great hope for what's to come in physics. We would also like to thank everyone who helped and made this internship possible.

References

[1] ON Semiconductor, *Introduction to the Silicon Photomultiplier (SiPM)*, Application Note AND9770/D, Rev. 9, August 2023. Available: https://www.onsemi.com/pub/Collateral/AND9770-D.PDF

[2] B. Sun, H. Li, Q. Li, H. Liang, C. Liu, H. Wang, Z. Wu, S. Xiao, and W. Xu, *Characterization of silicon photomultipliers for their application in muon scattering tomography*, Journal of Instrumentation, vol. 20, no. 02, p. T02003, Feb. 2025. Available: http://dx.doi.org/10.1088/1748-0221/20/02/T02003

[3] U.S. Department of Energy, *DOE Explains: Muons*, 2023. Available: https://www.energy.gov/science/doe-explainsmuons

[4] J. Pinto, M. Carvalho, and T. Paes, *Characterization of sealed RPC chambers subjected to a strong irradiation source*, LIP-STUDENTS-24-1, Oct. 2024.

[5] A. Blanco, J.Pinto *rpcReader – Readout and analysis software for RPC detectors*, GitHub repository, 2024. Available: https://github.com/albertoBlancoCastro/rpcReader

[6] ASUS, *RT-AX1800U – AX1800 Dual Band WiFi 6 Router*, Available: https://www.asus.com/pt/networking-iot-servers/wifi-routers/asus-wifi-routers/rt-ax1800u/